Two growth modes of graphitic carbon nanofibers with herring-bone structure

I. A. Merkulov,[1,*] A. V. Meleshko,[1] J. C. Wells,[2,†] H. Cui,[1] V. I. Merkulov,[1] M. L. Simpson,[1] and D. H. Lowndes[1]
[1]*Condensed Matter Sciences Division, Oak Ridge National Laboratory, Oak Ridge, Tennessee 37831-6016, USA*
[2]*Computer Science and Mathematics Division, Oak Ridge National Laboratory, Oak Ridge, Tennessee 37831-6016, USA*
(Received 7 March 2005; published 7 July 2005)

A simple mathematical model of the carbon nanofiber catalytic growth process is presented. Two major types of the fiber-catalyst interface shapes have been identified and described having qualitatively different structure in the center of a nanofiber. Presently, we discuss that the appearance of the irregular structure in the nanofiber central area is a result of curved-interface-growth kinematics. We suggest the method to determine the phenomenological parameters of the developed model from experimental data.

DOI: 10.1103/PhysRevB.72.045409 PACS number(s): 81.07.−b, 81.05.Uw, 68.65.−k, 81.16.−c

I. INTRODUCTION

Catalytic synthesis of carbon nanofibers (CNFs) has been studied since the 1950s.[1–8] From being an undesirable by-product, carbon nanofibers evolved to hold potential for a variety of applications such as cathodes for electron field emission sources,[9] scanning probe tips,[10,11] gene delivery media,[12] membranes,[13] and electrochemical sensors.[14] In particular, the expansion of possibilities for carbon nanofiber use can be attributed to the development of better control of their synthesis in a plasma enhanced chemical vapor deposition (PECVD) process.[15–17] While now the geometry of the nanofibers can be controlled with a higher degree of precision, the mechanisms that determine the internal crystal structure remain poorly understood.

In many cases, nanofibers structures consist of stacked cones of graphene sheets [Fig. 1(a)]. This is in contrast to carbon nanotubes (CNT), which consist of a single (or finite number) of graphene sheets rolled into perfect cylinders.[18] This type of structure of carbon nanofibers is usually labeled a herring-bone structure as its transmission electron microscopy (TEM) images resemble a fish skeleton. In the central region of these nanofibers, the regular structure of graphene layers is disrupted and spatial fluctuations are present in the carbon distribution (carbon bridges), including the occurrence of amorphous carbon regions and cavities. Sometimes the central region of the nanofiber is filled by the catalyst material.

In this work, we discuss the two types of herring-bone structures in catalytic CNF growth. In one case, a central orifice or cavity is separated from the stack of approximately conical surfaces by a region in which graphene layers are nearly parallel to the nanofiber growth direction [Fig. 1(b)]. Such a boundary region is suggestive of the carbon nanotube structure. In the second case, the similar transient region is absent and graphite layers terminate internally against the central nanofiber orifice [Fig. 1(c)]. Experimentally, we know that this central region may be occupied by amorphous carbon, metal catalyst, or remain unfilled. Within the phenomenological model developed here, the occurrence of two modes of herring-bone structure is the result of mutual nanofiber growth properties at curved graphite layers. The formal growth model considered here is characterized by phenomenological parameters that can be determined from experimental data.

II. GROWTH OF GRAPHITE FLAT SLAB

Our basic assumption is that the growth rate of graphitic material depends on its crystallographic orientation.[19,20] There are two different growth velocities V_n and V_t, normal to the graphene layer plane and in-plane, respectively. (Typically, $V_t \gg V_n$.) This growth anisotropy for CNF is well established by experimental evidence, and can be observed in recent *in situ* TEM images of CNF growth.[21] CNF growth occurs at the interface between the metal catalyst and the stacked graphene planes. In particular, in these recent TEM measurements, monoatomic steps are present at the catalyst surface and a graphene sheet terminates at each of these steps. Step-edge diffusion, leading to the in-plane growth of individual graphene layers, appears to occur at a rate greater than the spontaneous generation of new step edges at the interface, leading to the nucleation of new graphene layers. Moreover, the shape of the nanofiber is driven and in turn drives the shape of the catalyst particle at the interface during the growth process.[21]

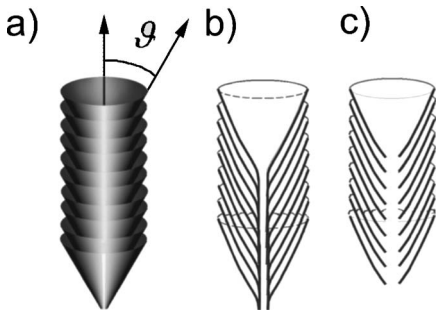

FIG. 1. Schematic herring-bone nanofiber structure: (a) Stack of graphene cones. (b) Nanofiber with inner cylindrical boundary within nanofiber creating a central orifice with zero tilt angle for the growth interface at this inner boundary (shown as a section along nanofiber axis). (c) The growth interface makes a finite tilt angle with the inner nanofiber boundary. The 2D cross sections shown in (b) and (c) have an orifice in the center of the nanofiber. (b) and (c) differ in the angle formed by the graphene sheet and the internal boundary of this orifice: the structure depicted in (b) has a smooth transition from the graphene sheet to the inner boundary; the structure depicted in (c) has an abrupt, nonzero angle of the graphene sheet and the inner boundary.

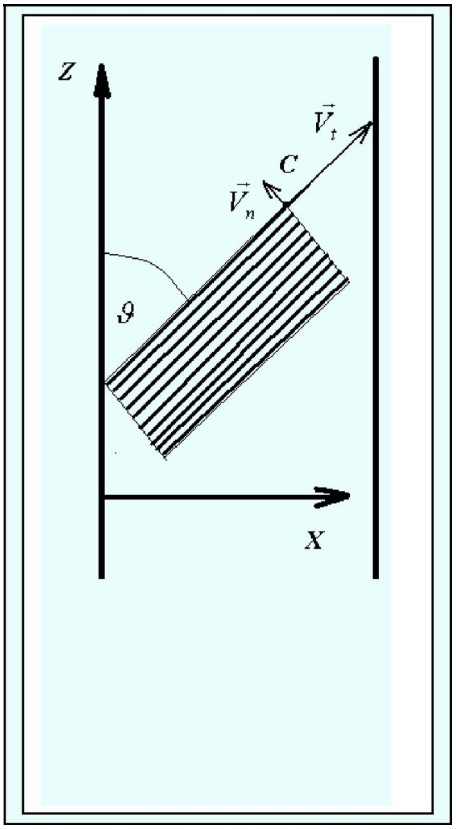

FIG. 2. (Color online) Anisotropic growth of a graphite slab constrained between two boundaries. The direction of motion of the corner point ***C*** is determined by the relation of the projection of normal $\vec{V}_n$ and tangential $\vec{V}_t$ growth rates onto the coordinate axis.

For purposes of illustration, let us also assume that growth of a slab of graphite occurs in space limited by two bounding planes and the angle between these planes and the plane graphene layers is ϑ (Fig. 2). The assumption of bounded growth is motivated by the experimental observation that the size of the catalytic particle limits the size, i.e., diameter, of the CNF. If the projection of the in-plane growth velocity V_t on the direction perpendicular to the bounding plane (i.e., the x direction in Fig. 2) is greater than the projection of the normal growth velocity V_n on the same direction, i.e.,

$$V_t \sin \vartheta > V_n \cos \vartheta, \tag{1}$$

then the graphene sheet edges will meet the bounding planes after finite time and growth will proceed only by stacking new graphene layers. The growth front will coincide with the plane of the graphene sheet and the growth rate along the Z axis will be $V_n/\sin \vartheta$. That is, the growth rate of the CNF will depend on V_n, and not on V_t. If the in-plane growth of the graphene layer toward the boundary is slower than the normal growth velocity projected toward the boundary,

$$V_n \cos \vartheta > V_t \sin \vartheta, \tag{2}$$

then the growth will proceed only due to (fast) deposition of carbon on the graphene edges, rather than the (slow) growth of the graphene layers. Finally, in the rare case when the two growth velocities projected on the x direction are equal, $V_n \cos \vartheta = V_t \sin \vartheta$, the growth front shape will be preserved in time. Thus the corner separating two surfaces—graphene sheet and the edges—shown in Fig. 2 will be propagated without a change. Extending the discussion from the flat slab of graphite shown in Fig. 2 to the curved, cylindrical surfaces, the former regime can be related to the growth of CNF and the later ($\vartheta < V_n/V_t \ll 1$) to CNT growth. In this present work, we are interested in the former case of CNF growth in which the vertical growth of the fiber depends on V_n, but not on V_t.

III. GROWTH RATES OF CURVED GRAPHITE

In the case of curved graphite, we need to introduce the corrections to the normal growth rate $V_{n,0}$ of a flat surface that can be deduced from symmetry considerations and the surface curvature (see, for example Ref. 22):

$$V_n(\vec{r}) = V_{n,0} - \Gamma_1 \sum_{m=1,2} \kappa_m - \Gamma_2 \sum_{m=1,2} \kappa_m^2 = \left(V_{n,0} + \frac{\Gamma_1^2}{2\Gamma_2} \right) - \sum_{m=1,2} \left(\frac{\Gamma_1}{2\Gamma_2} \vec{R}_m + \vec{n} \right)^2 \frac{\Gamma_2}{R_m^2}. \tag{3}$$

Here κ_m and $\vec{R}_m$ are two curvatures and two radii of curvature of a two-dimensional surface (i.e., graphene sheet) [$\kappa_m = (\vec{R}_m \vec{n})/R_m^2$] with indices $m=1$ or $m=2$. It is assumed that the vector radii point from the center of curvature toward the surface, i.e., curvatures of the growth front are negative for concave and positive for convex surfaces. The signs in Eq. (3) are chosen so that for positive values of the phenomenological parameters Γ_1, and Γ_2, and in the absence of additional limitations, the stable growth front remains flat. (The values of $V_{n,0}$, Γ_1, and Γ_2 are determined by growth conditions and could vary for different points on the growth front. Accounting for these variations is beyond the scope of this work.)

If one considers only terms up to those linear in the curvature in Eq. (3), the growth rate of concave surfaces is reduced compared to flat surfaces, while the growth rate of convex surfaces is increased. As a result, an oscillatory growth front tends to flatten. Considering terms up to those including the second-power of curvature, growth rates are reduced irrespective of the sign of the curvature. This effect is due to the fact that curved graphite layers are energetically unfavorable compared to flat layers. From the macroscopic point of view, the additional energy is due to elastic and plastic deformations.[23] From the microscopic standpoint, this excess energy is associated with bond bending and defects that appear in curved layers.[8]

Hence small bending toward concave shape increases growth rate and toward convex decreases it. Large bending always slows growth down and, at a certain value of curvature, completely stops it.

For convenience, let us use dimensionless variables, and express the normal growth rate of a flat surface $V_{n,0}$ and the growth rate of a curved surface $V_n(\vec{r})$ in units of $\Gamma_1^2/(4\Gamma_2)$,

$$v_n \equiv V_n \frac{4\Gamma_2}{\Gamma_1^2}, \quad v_{n,0} \equiv V_{n,0} \frac{4\Gamma_2}{\Gamma_1^2}, \tag{4}$$

and length in units of $2\Gamma_2/\Gamma_1$. Then Eq. (3) can be written as

$$v_n = (v_{n,0} + 2) - \sum_{m=1,2} (1 + \kappa_m)^2. \tag{5}$$

The maximum growth rate of

$$v_{n,\max} \equiv v_{n,0} + 2 \tag{6}$$

is reached at curvatures $\kappa_1 = \kappa_2 = -1$. More generally, the growth rate is the same for values of κ_m located on a circle with the center at coordinates $(-1,-1)$ and radius of curvature $\sqrt{v_{n,\max} - v_n}$. The curvature of the growth front completely determines the growth rate. With increasing absolute value of negative curvature, the growth rate initially increases and then decreases after passing through the maximum. Increasing absolute value of positive curvature leads to monotonous decrease of v_n. For given values of v_n and κ_1 (or κ_2), the value of the second curvature is expressed by the obvious relation

$$\kappa_{2,1} = -1 \pm \sqrt{v_{n,\max} - v_n - (1 + \kappa_{1,2})^2}. \tag{7}$$

A. Simple forms of curved graphite

The simplest shapes of curved graphite are represented by surfaces of constant curvatures, i.e., a sphere or part of a spherical surface. For spherical catalytic particles, the growth interface has uniformly constant curvature ($\kappa_1 = \kappa_2 = \kappa_s$), and

$$\kappa_{s,\pm} = -1 \pm \sqrt{\frac{v_{n,\max} - v_n}{2}}. \tag{8}$$

For a growing sphere ($\kappa_s > 0$), the curvature decreases as growth proceeds and the growth rate v_n will increase. For a graphitic sphere with curvature $\kappa_{s,+} = -1 + \sqrt{v_{n,\max}/2}$ the growth rate is equal to zero $v_n = 0$. This sphere is the critical seed size for the graphitic phase. For smaller radius, the sphere collapses. For larger radius, it grows. The spherical, negative-curvature cavity formed by the other side of the curved graphite slab ($\kappa < 0$) has curvature that converges to $\kappa_{s,-} = -1 - \sqrt{v_{n,\max}/2}$. This is a stable state. Larger cavities decrease in size and smaller cavities increase.

Using Eq. (5), it is also straightforward to analyze a cylindrical surface of graphite, $\kappa_2 = 0$,

$$\kappa_c = -1 \pm \sqrt{v_{n,0} + 1 - v_n}. \tag{9}$$

A graphitic rod with critical curvature

$$\kappa_{c,+} = r_{c,+}^{-1} = -1 + \sqrt{v_{n,0} + 1} \tag{10}$$

is unstable and the negative curvature cavity with curvature

$$\kappa_{c,-} = -r_{c,-}^{-1} = -1 - \sqrt{v_{n,0} + 1} \tag{11}$$

is stable.

In the following we will conduct an analysis of more complex surface shapes that model real interfaces in carbon nanofibers.

B. Steady state growth front

In order to use the formulas presented above for analysis of the catalytic synthesis of carbon nanofibers, it is necessary to know the values of the parameters $V_{n,0}$, Γ_1, and Γ_2 at the interface between the catalyst particle and the nanofiber. These phenomenological parameters are determined by many factors that cannot be calculated within the models presented in this paper. We will limit ourselves to the analysis of a simple model problem. Let us assume that the values of parameters $V_{n,0}$, Γ_1, and Γ_2 are the same everywhere along the interface, i.e., we will not take into account nonuniformity of growth conditions due to external processes such as diffusion, catalyst stresses, etc. As a main control parameter of the system under investigation, we will consider the total growth rate of a nanofiber in steady-state conditions $V_z = v_z \Gamma_1^2/(4\Gamma_2)$. The relation of this parameter to the initial conditions of the problem is not obvious. Therefore, for our model problem, let us consider the situation of steady-state growth of a cylindrically symmetric nanofiber along the vertical (i.e., z) direction for the relatively simple situation of normal interface growth rate depending only on the local curvature, as in Eq. (5). If the tilt angle of the graphene sheets is not large (1), the shape of the interface is given by

$$v_z = \frac{v_n[r, \vartheta(r)]}{\sin \vartheta(r)}, \tag{12}$$

where r is the radial distance from the axis of symmetry, $\vartheta(r)$ is the local, polar, or tilt angle defined relative to the z direction, and $v_n[r, \vartheta(r)]$ is the local normal interface growth rate (5). For cylindrical nanofibers, the two curvatures at the point r at the interface are

$$\kappa_1(r) = \pm \frac{\cos \vartheta(r)}{r}, \tag{13}$$

$$\kappa_2(r) = \pm \frac{d[\cos \vartheta(r)]}{dr}. \tag{14}$$

The signs in Eqs. (13) and (14) depend on which side of the interface carbon is deposited. For geometries considered in Figs. 1(b) and 1(c) $0 < \vartheta < \pi/2$ and in Eqs. (13) and (14) the negative signs should be used. The functional dependence of the shape or form of the growth interface, $Z(r)$, can be related to the tilt angle as follows:

$$\frac{dZ(r)}{dr} = \frac{\cos \vartheta(r)}{\sin \vartheta(r)}. \tag{15}$$

For a continuous and smooth surface, cylindrical symmetry implies that if the surface is present at the center of the nanofiber, then at $r = 0$ the surface is normal to the growth direction $\vartheta(r=0) = \pi/2$, and $\kappa_1(0) = \kappa_2(0) = \kappa(0)$. The value of $\kappa(0)$ is given by Eq. (8) in which $v_n \equiv v_z$. Obviously, this boundary condition can be satisfied only for small values of the total growth rate ($v_z \leqslant v_{n,\max}$).

By substituting Eqs. (13) and (14) in Eq. (7), we obtain two possible equations,

$$\frac{d\cos\vartheta}{dr} = 1 \mp \sqrt{v_{n,\max} - v_z \sin\vartheta - \left(1 - \frac{\cos\vartheta}{r}\right)^2}. \tag{16}$$

The coupled differential equations (15) and (16) constitute the formal, mathematical model for the calculation of the interface form, $Z(r)$. For small r, the solutions (16) that satisfy the boundary condition (8) are

$$\cos\vartheta \approx \left(1 \mp \sqrt{\frac{v_{n,\max} - v_z}{2}}\right) r. \tag{17}$$

We note that due to the nonlinearity of the problem, the superposition principle does not apply and we cannot obtain a general solution as linear combinations of solutions of the form (17). However, we can match different solutions within different regions of the interface. In further analysis, we will restrict ourselves to only positive values $v_z \geqslant 0$ that correspond to growth of a nanofiber.

If $v_z = 0$, the solutions (17) are valid in a large range of values of r. The interface in this case is a part of a sphere with critical value of curvature $\kappa_{s,\pm}$. The interface that corresponds to the use of the minus sign in Eq. (16) is displayed in the left part of Fig. 3(a), and the plus sign is displayed on the right side. The "−" solution in this case corresponds to positive curvature of the interface and the "+" solution to negative curvature. The interface function $Z(r)$ is obtained by successively integrating Eqs. (16) and (15). An example using $v_{n,0}=1, v_z=0$ is presented in Fig. 3(a).

Increasing the growth rate only weakly affects the shape of the "+" interface and abruptly decreases the curvature of the "−" solution. (Notice the change in the interface, displayed in Fig. 3(b), when using $v_{n,0}=1, v_z=0.9$.) For $v_z = v_{n,0}$, the "−" solution corresponds to a flat interface $\kappa_{1,2} = 0$, and the maximal possible value of the nanofiber radius $\tilde{r}^{(-)}_{\max}(v_{n,0} \leqslant v_z)$ becomes infinity. The characteristic radius for the "+" solution remains on the order of $\kappa^{-1}_{s,-}$.

If $v_z > v_{n,0}$, then both "−" and "+" solutions correspond to interfaces with negative curvature. From Eqs. (13) and (14), both the curvatures of the "−" solution approach zero with increasing r. From the asymptotic $r \to \infty$ solution to Eq. (16), we obtain the asymptotic value of the tilt angle of the interface with respect to the axis of the fiber

$$\lim_{r\to\infty}[\sin\vartheta(r)] = v_{n,0}/v_z. \tag{18}$$

These conditions correspond to the formation of nanofibers with herringbone structure. When v_z reaches its maximum $v_z = v_{n,\max} = v_{n,0} + 2$, the square root in the boundary condition (17) becomes zero. The curvatures of both "+" and "−" interfaces at $r=0$ are the same and equal to -1, [e.g., see Fig. 3(c)]. Increasing the growth rate further, i.e., $v_z > v_{n,\max}$, requires violating the assumptions of a continuous and smooth surface, as the argument of the cosine function in Eq. (17) becomes imaginary. One way in which the growth rate may increase beyond $v_{n,\max}$ is for continuity to be sacrificed and a void or orifice to open at the center of the fiber. Indeed, it follows from the analysis of Eq. (16) that $|\sin\vartheta| < v_{n,\max}/v_z$ for all points of the interface. This condition can be satisfied with a cylindrically symmetric interface and $v_z > v_{n,\max}$ only away from the center of the nanofiber, $r > 0$. Therefore the growth interface should have an inner, as well as an outer, cylindrical boundary surface, which develops over time during the growth process. Some features of this solution can be determined from the following simple considerations.

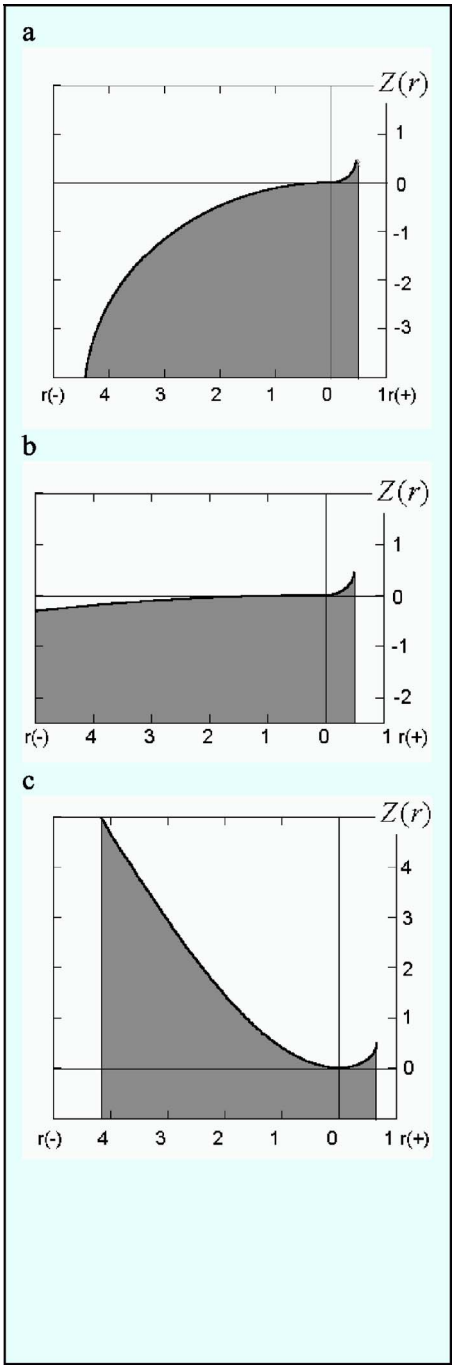

FIG. 3. (Color online) Evolution of growth interface shape for "+" ($r^{(+)}$) and "−" ($r^{(-)}$) solution of the coupled equations (15) and (16): (a) $v_{n,0}=1, v_z=0$; (b) $v_{n,0}=1, v_z=0.9$; and (c) $v_{n,0}=1, v_z=3$. The dark region represents the presence of the nanofiber.

Assuming that the second curvature is small ($\kappa_2 \ll 1$), we can omit terms containing κ_2 in Eqs. (5), (7), and (16). For this approximation, the tilt angle and radius of the interface are connected by the following equation, in which the inter-

face radius r_0 is expressed, for present purposes, as a function of the tilt angle.

$$r_0(\vartheta) = \frac{\cos\vartheta}{1 \pm \sqrt{v_{n,0} + 1 - v_z \sin\theta}}. \tag{19}$$

We are only interested in positive tilts ($0 < \vartheta < \pi/2$) and radii ($r_0 > 0$).

Let us find out how the value of κ_2 influences the interface shape, or equivalently, take into consideration the derivative of the interface tilt angle with respect to the radius (14). At the internal nanofiber boundary surface, r_{int}, the graphene-catalyst interface is terminated by some means. From the point of view of this analysis, Eq. (16) does not have real-valued solutions for $r < r_{\text{int}}$. But, for $r \geqslant r_{\text{int}}$, such solutions exist, and can be classified by their behavior at r_{int}. In one class, the growth interface at $r = r_{\text{int}}$ forms a zero tilt angle with the internal nanofiber boundary [e.g., see, for illustration, Fig. 1(b)], and the growth interface at $r = r_{\text{int}}$ has zero velocity, i.e.,

$$\vartheta(r_{\text{int}}) = 0,$$

$$v_n(r_{\text{int}}) = v_{n,0} + 2 - \left(1 - \frac{1}{r_{\text{int}}}\right)^2 - \left(1 - \left.\frac{d\cos\vartheta}{dr}\right|_{r=r_{\text{int}}}\right)^2 = 0,$$

$$\left.\frac{d\cos\vartheta}{dr}\right|_{r=r_{\text{int}}} < 0. \tag{20}$$

In another class of solutions, the square root in Eq. (16) is equal to zero at the radius $r = r_{\text{int}}$. In this case, the growth interface at $r = r_{\text{int}}$ makes a finite angle with the internal nanofiber boundary, i.e.,

$$\left.\frac{d\cos\vartheta}{dr}\right|_{r=r_{\text{int}}} = 1,$$

$$r_{\text{int}} = \frac{\cos\vartheta_{\text{int}}}{1 \pm \sqrt{v_{n,0} + 2 - v_z \sin\vartheta_{\text{int}}}} \geqslant 0. \tag{21}$$

Figures 4(a) and 4(b) show examples of the radial dependence of the interface tilt angles $\vartheta(r)$, and Figs. 5(a) and 5(b) show examples of the interface shapes, each calculated from Eqs. (16), (20), and (21) and for two values of growth rates $v_{n,0}=1$, $v_z=3$ and $v_{n,0}=1$, $v_z=4$. The dashed line in Figs. 4 and 5 corresponds to the approximate equation (19), for which the second principle curvature is assumed negligible. Curves labeled 1, 2, 3, and 4 are constructed for boundary conditions (21) with sign "+" before square root, and curves 5, 6, and 7 are constructed for boundary condition (21) with sign "−". Curves 8, 9, 10, and 11 are constructed for boundary conditions (20). One can see that the second curvature κ_2 strongly influences the relationship between the radial position of the internal nanofiber boundary and the interface tilt angle near the internal boundary. In this region, interface solutions described by the boundary conditions (20) form a series of solutions falling below the approximate interface (19). On the contrary, interfaces described by conditions (21) fall above the approximate interface (19) and are characterized by large values of the angle ϑ near the inner nanofiber boundary. The role of κ_2 is more significant at small values of the nanofiber growth rate just beyond the threshold for the appearance of the central cavity. The disappearance of the orifice at lower growth rates, i.e., $0 < v_z \leqslant v_{n,0} + 2$ is possible only for boundary conditions (21) and $\kappa_2 \neq 0$. One can see that interface solutions corresponding to boundary conditions (21) have spherical geometry of the growth interface, i.e., the

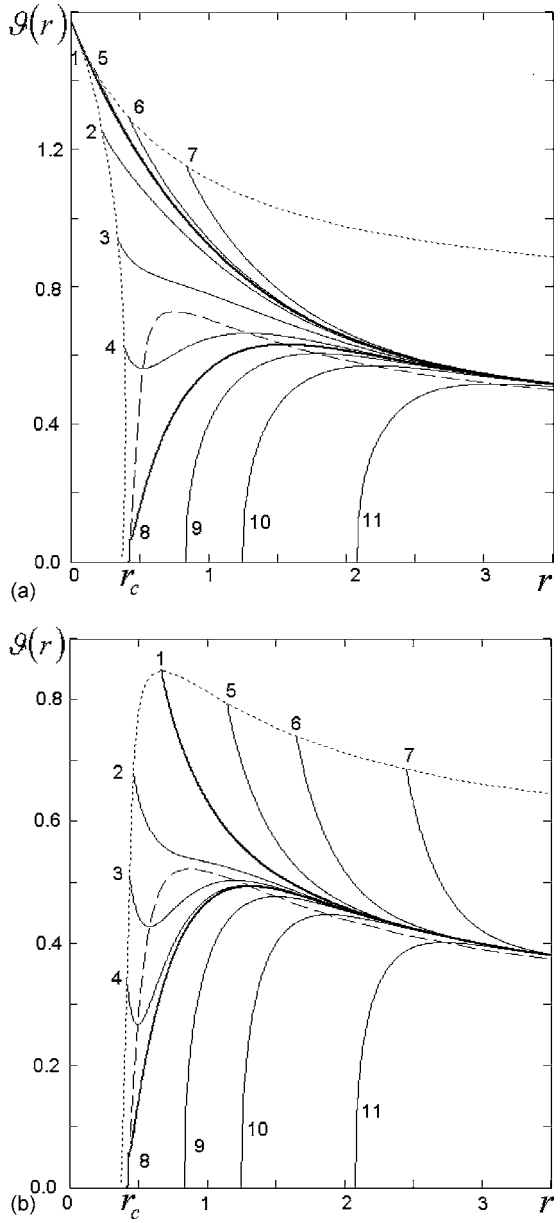

FIG. 4. Radial dependence of interface tilt angle, $\vartheta(r)$, for a given, asymptotic $\lim_{r\to\infty} \sin\vartheta(r) = v_{n,0}/v_z$ tilt-angle dependence: (a) $v_z = v_{n,0} + 2 = 3$ and (b) $v_z = 4, v_{n,0} = 1$. Curves 1–4 are constructed for boundary conditions (21) with sign "+" before square root, and curves 5–7 are constructed for boundary condition (21) with sign "−." Curves 8–11 are constructed for boundary conditions (20). The dashed line corresponds to the approximate equation (19). From the experimental observation of the two special interface forms 1 and 8 described within the text and depicted with bold lines, one can obtain values of the major phenomenological parameters of our kinetic model.

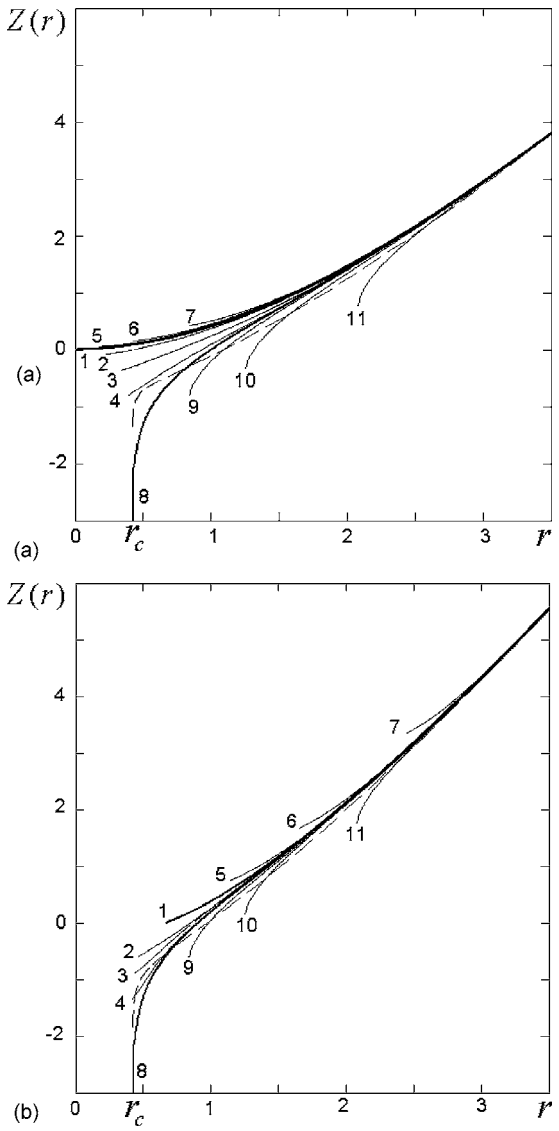

FIG. 5. The shape of the nanofiber growth interface as a function of the radial distance, for a given asymptotic $\lim_{r\to\infty} \sin\vartheta(r) = v_{n,0}/v_z$ tilt-angle dependence: (a) $v_z = v_{n,0} + 2 = 3$ and (b) $v_z = 4, v_{n,0} = 1$. The in-figure notation is identical to that used in Fig. 4.

product of the two principle curvatures is positive. For boundary conditions (20), the interface geometry is spherical at the outer regions of the nanofiber, but in the inner region it is hyperbolic.[8] Examples of structures corresponding to Eq. (20) can be found as TEM images given in Ref. 24, and in Fig. 2 and *in situ* TEM "movie" N1 from the supplementary information in Ref. 21 Interfaces satisfying (21) may be observed, for example, in the TEM images published in Ref. 25 and in the second *in situ* TEM "movie" N2 from supplementary information published with Ref. 21.

The nonzero value of κ_2 allows for the variation of the central orifice diameter over a wide range of values. From Fig. 4, one can see that for the high value of growth rate the different interfaces have practically the same shapes and differ only in the central orifice diameter.

From a large number of possible interfaces, we have selected two interfaces that correspond to special conditions. One interface with special significance corresponds to boundary conditions (21) and is that with maximum possible tilt angle at the inner boundary $\vartheta(r_{\text{int}}) \equiv \vartheta_{\max} = \arcsin(v_{n,\max}/v_z)$ [Eq. (12)]. The bold line with label 1 corresponds to this special interface in Figs. 4 and 5. The second interface of special significance is that which possesses the minimum value for the radius of the central cavity. This interface is presented by a bold line in Figs. 4 and 5 with label 8, and is identified with the class of boundary conditions (20). In this case, the radius of the central cavity is equal to $r_1 \equiv r_{c,-}$ and connected with $v_{n,0}$ by formula (11). At the internal nanofiber boundary $\kappa_1(r_{\text{int}}) = \kappa_2(r_{\text{int}}) = -1$ and the value of the dimensionless radius of the central orifice is directly connected with the experimentally determined value of the tilt angle at the inner boundary:

$$r_2 = \cos\vartheta_{\max}. \tag{22}$$

Thus by measuring $\vartheta_{\max}$ and the corresponding radius of the internal orifice $(r_2 L_0)$, one can determine the natural length unit $L_0 = 2\Gamma_2/\Gamma_1$. After this, the experimental measurement of the size of the central cavity in herring-bone nanofibers $r_1 L_0$ will allow one to estimate the dimensionless rate $v_{n,0}$. This rate is connected with the dimensionless nanofiber growth rate v_z by Eq. (18). Then, by measurement of the interface tilt angle far from the central cavity, one can calculate v_z. By comparing v_z with the experimental value for the nanofiber growth rate $V_z = v_z(\Gamma_1^2/4\Gamma_2)$, one can obtain values of all phenomenological parameters of this model.

IV. DISCUSSION

The kinematical model developed here describes the major, qualitative, and significant features of steady state, catalytic carbon-nanofiber growth. As in any kinematical model, it does not include a discussion of the forces, processes, or mechanisms causing this growth. For example, we considered the growth rate v_z as the master parameter determining the growth front shape. Alternatively, the angle of the conical interface at large distances, $\vartheta(r \to \infty)$, may be taken as a master parameter. This angle is directly related with v_z and $v_{n,0}$ by Eq. (18). As discussed in Refs. 26–28 the angle $\vartheta(r \to \infty)$ may be connected with the hydrogen-plasma concentration as well as with the orientation of the crystalline metal catalyst. Such rearrangement of reasons and consequences does not affect the major results of the analyses provided here and the experimental determination of phenomenological model parameters.

The assumption of the spatial uniformity of the growth conditions and constant values of phenomenological parameters along the interface has a much larger influence on the quantitative agreement of the present calculations with experimental data. For example, one can imagine that the dependence of the growth rate on the catalytic film thickness, i.e., due to variation of diffusion distance, leads to the sign change of the parameter Γ_1 and thus to instability of the flat growth front.

The availability of experimental information about distributions of values of the phenomenological parameters used in this work would be very useful for the development of a more complete process description.

V. CONCLUSION

In conclusion, we summarize the major results of this investigation.

(1) The presented kinematic model of the catalytic carbon-nanofiber growth considers the dependence of the normal rate of growth (V_n) on the surface curvature of the growth interface. The model allows for the understanding of how the growth front shape (the interface between the carbon nanofiber and the catalyst) changes with the normal growth rate.

(2) There are two types of the interface growth that drastically differ in the angle between the graphene sheet and the nanofiber axis near the center of the fiber (small radial values). In one case, at small growth rates, the interface exists in the nanofiber center ($r=0$) and is perpendicular to the growth direction. In the second case, even at small growth rates, an internal, cylindrical nanofiber boundary exists at $r_{\text{int}} \neq 0$, producing a cavity in the nanofiber center. The interface tilt far from the center is simply related to the ratio of the growth rate v_z and the characteristic rate $v_{n,0}$. For large growth rates, the presence of the central cavity is consistent with both interface types. This central cavity may be empty, filled by catalyst, graphite bridges, amorphous carbon, etc., and our kinematic model does not distinguish among these scenarios.

(3) We have also shown that the central cavity diameter varies over a wide range of values. Based on the experimental dependence of the interface angle at the inner boundary $\vartheta(r_{\text{int}})$ and the central cavity radius r_{int}, it is possible to determine the major, phenomenological growth parameters of a herring-bone nanofiber structure.

ACKNOWLEDGMENTS

I. A. Merkulov and V. I. Merkulov give thanks to G. Y. Merkulov for encouraging discussions and help. Our research was sponsored by the Division of Materials Sciences and Engineering, U.S. Department of Energy (USDOE) under Contract No. DE-AC05-00OR22725 with UT-Battelle, LLC.

*On leave from loffe Physico-Technical Institute, Russian Adademy of Sciences.

†Corresponding author.

[1] L. V. Radushkevich and V. M. Lukyanovich, Zh. Fiz. Khim. **26**, 88 (1952).

[2] R. T. K. Baker, Carbon **27**, 315 (1989).

[3] N. M. Rodriguez, J. Mater. Res. **8**, 3233 (1993).

[4] N. M. Rodriguez, A. Chambers, and R. T. K. Baker, Langmuir **11**, 3862 (1995).

[5] K. P. De Jong and J. W. Geus, Catal. Rev. - Sci. Eng. **42**, 481 (2000).

[6] *Carbon Nanotubes: Synthesis, Structure, Properties, and Applications*, edited by M. S. Dresselhaus, G. Dresselhaus, and P. Avouris, *Topics in Applied Physics*, Vol. 80 (Springer, Berlin, 2001).

[7] H. J. Dai, Surf. Sci. **500**, 218 (2002).

[8] H. Terrones and M. Terrones, New J. Phys. **5**, 1 (2003).

[9] M. A. Guillorn, X. J. Yang, A. V. Melechko, D. K. Hensley, M. D. Hale, V. I. Merkulov, M. L. Simpson, L. R. Baylor, W. L. Gardner, and D. H. Lowndes, J. Vac. Sci. Technol. B **22**, 35 (2004).

[10] Q. Ye, A. Cassell, H. Liu, K.-J. Chao, J. Han, and M. Meyyappan, Nano Lett. **4**, 1301 (2004).

[11] H. Cui, S. V. Kalinin, X. Yang, and D. H. Lowndes, Nano Lett. **4**, 2157 (2004).

[12] T. E. McKnight, A. V. Melechko, D. K. Hensley, D. G. J. Mann, G. D. Griffin, and M. L. Simpson, Nano Lett. **4**, 1213 (2004).

[13] B. L. Fletcher, E. D. Hullander, A. V. Melechko, T. E. McKnight, K. L. Klein, D. K. Hensley, J. L. Morrell, M. L. Simpson, and M. J. Doktycz, Nano Lett. **4**, 1809 (2004).

[14] J. Li, H. T. Ng, A. Cassell, W. Fan, H. Chen, Q. Ye, J. Koehne, J. Han, and M. Meyyappan, Nano Lett. **3**, 597 (2003).

[15] M. Chhowalla, K. B. K. Teo, C. Ducati, N. L. Rupesinghe, G. A. J. Amaratunga, A. C. Ferrari, D. Roy, J. Robertson, and W. I. Milne, J. Appl. Phys. **90**, 5308 (2001).

[16] Z. F. Ren, Z. P. Huang, J. W. Xu, J. H. Wang, P. Bush, M. P. Siegal, and P. N. Provencio, Science **282**, 1105 (1998).

[17] V. I. Merkulov, D. K. Hensley, A. V. Melechko, M. A. Guillorn, D. H. Lowndes, and M. L. Simpson, J. Phys. Chem. B **106**, 10570 (2002).

[18] S. Iijima, Nature (London) **354**, 56 (1991).

[19] E. C. Frank, in *Growth and Perfection of Crystals*, edited by R. H. Doremus, B. W. Roberts, and D. Turnbull (Wiley, New York, 1958).

[20] A. A. Chernov, *Modern Crystallography III, Crystal Growth* (Springer-Verlag, Berlin, 1984), p. 122.

[21] S. Helveg, C. López-Cartes, J. Sehested, P. L. Hansen, B. S. Clausen, J. R. Rostrup-Nielsen, F. Abild-Pedersen, and J. K. Nørskov, Science **427**, 426 (2004).

[22] R. C. Brower, D. A. Kessler, J. Koplik, and H. Levine, Phys. Rev. Lett. **51**, 1111 (1983).

[23] G. G. Tibbetts, J. Cryst. Growth **66**, 632 (1984).

[24] M. H. Kuang, Z. L. Wang, X. D. Bai, J. D. Guo, and E. G. Wang, Appl. Phys. Lett. **76**, 1255 (2000).

[25] H. T. Cui, X. J. Yang, M. L. Simpson, D. H. Lowndes, and M. Varela, Appl. Phys. Lett. **84**, 4077 (2004).

[26] A. Krishnan, E. Dujardin, M. M. J. Treacy, J. Hugdahl, S. Lynum, and T. W. Ebbesen, Nature (London) **388**, 451 (1997).

[27] P. E. Nolan, D. C. Lynch, and A. H. Cutler, J. Phys. Chem. B **102**, 4165 (1998).

[28] H. Terrones, T. Hayashi, M. Munoz-Navia, M. Terrones, Y. A. Kim, N. Grobert, R. Kamalakaran, J. Dorantes-Davila, R. Escudero, M. S. Dresselhaus, and M. Endo, Chem. Phys. Lett. **343**, 241 (2001).